Journal of Cleaner Production 461 (2024) 142673

Contents lists available at ScienceDirect

Journal of Cleaner Production

journal homepage: www.elsevier.com/locate/jclepro

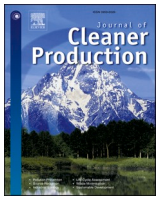

Novel cesium immobilization by alkali activation and cold consolidation of waste pharmaceutical glass

Diana Lago [a], Giulia Tameni [b], Federico Zorzi [c], Jozef Kraxner [a], Dušan Galusek [a,d], Enrico Bernardo [b,*]

[a] FunGlass – Centre for Functional and Surface Functionalized Glass, Alexander Dubček University of Trenčín, Študentská 2, 911 50, Trenčín, Slovakia
[b] Department of Industrial Engineering, University of Padova, Via Marzolo 9, 35131, Padova, Italy
[c] Centro di Analisi e Servizi per la Certificazione (CEASC), University of Padova, Via Jappelli 1/A, 35131, Padova, Italy
[d] Joint Glass Centre of the IIC SAS, TnUAD and FChFT STU, 911 50, Trenčín, Slovakia

ARTICLE INFO

Handling Editor: Mingzhou Jin

Keywords:
Alkali activation
Boro-pollucite
Cesium immobilization
Cold consolidation process
Viscous flow sintering

ABSTRACT

A new method of cesium immobilization has been successfully developed by combining alkali activation of boro-alumino-silicate glass and viscous flow sintering. Powdered glass from discarded pharmaceutical vials, suspended in a 2.5 M CsOH aqueous solution, underwent surface hydration as well as partial dissolution. Condensation reactions occurring at hydrated surface layers upon drying at 40 °C over 7 days resulted in welding of adjacent particles, forming a network that trapped newly formed gel and crystal phases. The newly formed phases including crystalline boro-pollucite ($CsBSi_2O_6$), were derived mostly from Cs^+ ions reacting with the products of glass dissolution and exhibited a high chemical stability. Further stabilization was achieved through viscous flow sintering at 700 °C, resulting in the incorporation of Cs^+ ions in a glass matrix. The effectiveness of the immobilization was confirmed by leaching test using the Materials Characterization Center-1 Standard (MCC-1). This innovative approach not only enhances the chemical stability of cesium waste forms, but also aligns with principles of cleaner production by repurposing pharmaceutical glass waste, promoting sustainable materials management.

1. Introduction

Electric power generation is crucial for development and growth of global economies. There is a global trend toward implementing environmentally friendly production and sustainability policies. This is emphasized by the sustainable development goals set during the recent United Nations Conference on Climate Change in Glasgow (COP26), which call for all countries to promote prosperity while protecting the planet, (Hunter et al., 2022).

In countries where nuclear energy is included in the energy matrix, great potential for decarbonisation is envisaged by the gradual replacement of fossil fuels (Zou et al., 2021). Nuclear power plant (NPP) emit an average of 23 g CO_2/kWh over their complete life cycle (30–40 years). This emission rate is comparable to that of wind energy plants and significantly lower than that of solar energy plants (30–50 g CO_2/kWh) (Pomponi and Hart, 2021). However, the generation of radioactive waste remains a significant concern and constitutes one of the main barriers to the life extension of NPPs.

The overall sustainability of NPPs depends on an effective and sustainable process of waste stabilization: in this regard, glass represents a reference material. Vitrification is one of the most widely used treatments for high-level radioactive wastes (HLW) (Ojovan et al., 2021) and borosilicate glass is internationally recognized as the most suitable host matrix. However, radioactive waste is fixed in the glass structure only by a high-temperature treatment that consists of melting or sintering of glass powders mixed with radioactive waste particulates (Lago et al., 2022).

Some radionuclides are particularly complicated to manage due to their intrinsic complexity, such as long half-life, high activity, solubility in water, and high volatility even at low temperatures. One of the radionuclides possessing all these properties and therefore presenting a great physical-chemical and radiological complexity during immobilization is cesium. Cesium has over 30 isotopes; whilst ^{133}Cs is the only one naturally occurring stable isotope, $^{134,135,136,137}Cs$ isotopes are all

* Corresponding author.
E-mail addresses: diana.lago@tnuni.sk (D. Lago), giulia.tameni@phd.unipd.it (G. Tameni), federico.zorzi@unipd.it (F. Zorzi), jozef.kraxner@tnuni.sk (J. Kraxner), dusan.galusek@tnuni.sk (D. Galusek), enrico.bernardo@unipd.it (E. Bernardo).

https://doi.org/10.1016/j.jclepro.2024.142673
Received 6 October 2023; Received in revised form 21 May 2024; Accepted 23 May 2024
Available online 24 May 2024
0959-6526/

radioactive (Caurant et al., 2007). In HLW, cesium radioactivity during the first three centuries is determined primarily by ^{137}Cs due to its relatively short half-life (30 y). Later, the dominant contribution is due to ^{135}Cs which has an extremely long half-life ($2.3{\cdot}10^6$ y, Fig. 1).

The solubility in water makes cesium isotopes an essential component of nuclear wastewater. Various methods of cesium removal were developed, including ion exchange, membrane separation, and solvent extraction (Wang and Zhuang, 2020). The process relies on the use of zeolite minerals as sorbents. Zeolites are alumino-silicate compounds with a three-dimensional network structure based on the bridging of SiO_4 and AlO_4 units. The latter are typically stabilized by alkaline ions, which can be exchanged with cesium cations (Bosch et al., 2004). After cesium incorporation, it is essential to seal the structure to avoid cesium leaching in case zeolite comes back into contact with water. Li et al. observed that high-temperature sintering of Cs-loaded zeolite leads to the formation of ceramics based on crystalline cesium feldspar (pollucite, $CsAlSi_2O_6$, i.e. $Cs_2O{\cdot}Al_2O_3{\cdot}4SiO_2$) (Li et al., 2022). Gatta et al. synthesized crystalline $CsAlSiO_4$ from a stoichiometric mixture of Al_2O_3, SiO_2 and Cs_2O, employing extreme synthesis conditions, including a hydrostatic pressure of 0.1 GPa, a temperature of 695 °C, and a synthesis duration of 46 h (Gatta et al., 2008). Due to its framework structure, which features six rings with shared oxygens from the $(Al, Si)O_4$ tetrahedra, pollucite has a high chemical stability (He et al., 2019). The diameter of cesium ions (3.34 Å) is larger than the diameter of the six ring (2.8 Å), making it impossible for cesium ions to escape the framework (He et al., 2019).

Several works suggest that pollucite is one of the most stable phases for cesium immobilization (Omerašević et al., 2020; Feng et al., 2023). However, after adsorption, this process requires vitrification of the cesium-containing zeolite for long-term disposal in geological repositories (Omerašević et al., 2020).

Beyond the ion exchange of zeolites, pollucite can be synthesized by hydrothermal treatment (Liu et al., 2021) or from geopolymer precursors (Tian et al., 2022). High-temperature treatments involve heating up to 1000–1200 °C; the processing temperature may be downscaled to about 800 °C only by hot-pressing (Omerašević et al., 2020). Since many cesium compounds are characterized by a high vapor pressure even at low temperatures (≥400 °C), the probability of cesium loss by volatilization remains high. The use of geopolymeric precursors requires much lower temperatures (150–300 °C) but also exact conditions of formulation (Feng et al., 2023).

Geopolymers belong to a vast family of alkali-activated materials. Highly concentrated aqueous solutions of alkali silicates, aluminates, or hydroxides are designed to attack alumino-silicate feedstock, resulting in the release of 'sialate' oligomers, into the solution. In a subsequent step, these oligomers form a three-dimensional network structure, by a series of condensation reactions (Davidovits, 2011), upon drying below 100 °C. The network structure, although amorphous, has an evident analogy with zeolites in the bridging (by shared oxygens) of SiO_4 and AlO_4 units, the latter being stabilized by the alkaline ions originating from the attacking solution (Provis, 2014). The chemical stability of the obtained 'zeolite-like' gel, resulting from Si–O–Si and Si–O–Al bonds, is the key to the stabilization of heavy metals (El-Eswed, 2020); radionuclides represent an additional extension.

Alkali activation can also be applied to glass. Several investigations have suggested that pulverized waste glasses could be dissolved easily and release silica-rich species under alkaline conditions due to their large surface area and amorphous nature (Liu et al., 2019; Xiao et al., 2020). Alkali-activated materials have been also explored as the next generation of environmentally sustainable binding materials, because of their lower carbon footprint when compared to industrial cementitious materials. The eco-friendly approach of alkali-activated materials is also related to the use of various alumino-silicate wastes (Xiao et al., 2022).

When reacted with concentrated alkaline solutions, alumino-silicate glass powders are also useful precursors of (semi-crystalline) zeolite-like gels (Garcia-Lodeiro et al., 2014). Recent studies have also demonstrated the potential of 'mild' alkaline solutions (NaOH molarity not exceeding 3 M) in the activation of discarded glasses (Idir et al., 2020; Ramteke et al., 2021). Among waste glasses, the boro-alumino-silicate glass from discarded pharmaceutical vials is of particular interest (Mehta et al., 2022): mild activation leads to the bonding of adjacent unreacted particles through thin surface layers. Upon drying at 40–80 °C ('cold consolidation'), adjacent particles are 'welded' by the condensation of Si–OH, B–OH, and Al–OH terminal groups at the surface (Fig. 2). The components released into the solution that are not involved in the formation of bridges between adjacent particles remain physically trapped between the same particles, forming a gel (Lago et al., 2023). The interactions between alkali and the atmosphere yields hydrated alkali carbonates. The carbonates are easily removed by placing samples in boiling water; the gel, likely due to limited network connectivity, is dissolved as well (Lago et al., 2022). The integrity of samples after the removal of soluble phases may be seen as the proof of the establishment of strong bonds between glass particles (Tameni et al., 2022).

The present study is aimed at the application of alkali activation of pharmaceutical glass to the immobilization of cesium. The main novelty lies in the use of a CsOH diluted solution, with a double purpose. Firstly, the activation confirms the cold consolidation observed with NaOH and KOH treatment. Secondly, the release of the components of glass into the solution is an opportunity to synthesize a phase structurally similar to pollucite mentioned above (Bubnova et al., 2004). A final stabilization by viscous flow sintering promotes the dissolution of the pollucite solid solution and immobilization of Cs^+ ions into a new stable amorphous material.

2. Experimental procedure

The starting material consisted of boro-alumino-silicate glass (BASG) cullet obtained from discarded pharmaceutical vials. This particular cullet, supplied by Stevanato Group, Piombino Dese, Italy was considered 'dirty' production waste due to the presence of traces of oil. The

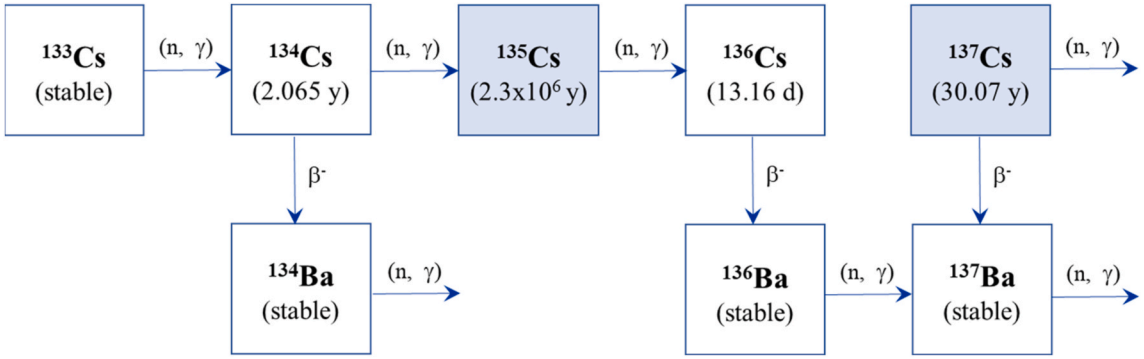

Fig. 1. Radioactive decay diagram of cesium, (Ojovan et al., 2019).

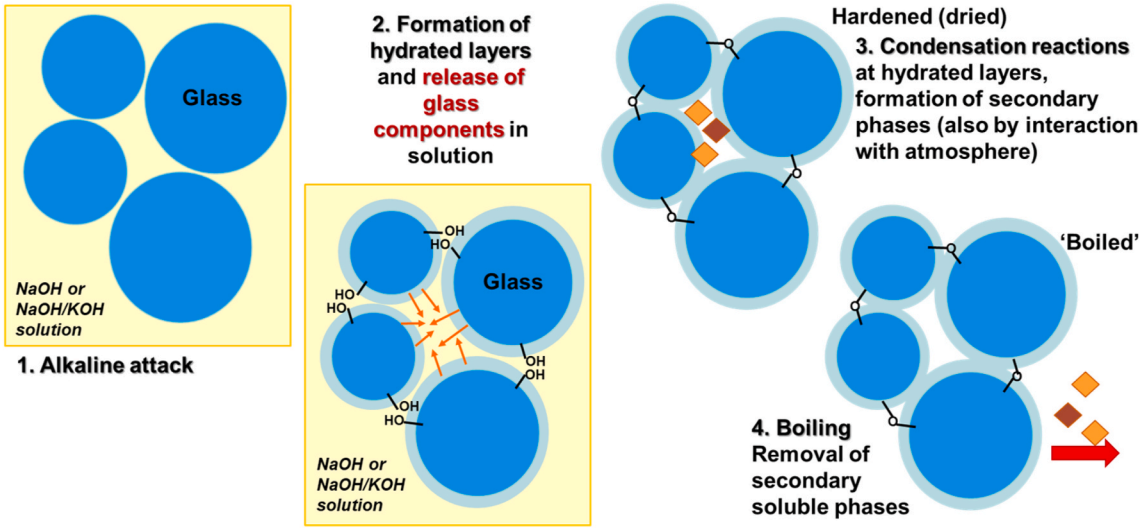

Fig. 2. Schemes of alkali activation and cold consolidation from NaOH or NaOH/KOH solution.

fragments of glass vials were crushed and milled in a planetary mill (Pulverisette 6, Fritsch GmbH, Idar-Oberstein, Germany). For the milling procedure, agate balls with a diameter of 15 mm were employed, maintaining a powder-to-ball mass ratio of 1:25. The small glass pieces were milled three times for 30 min at a rotation speed of 300 rpm. The milled powder was sieved to obtain particles with a size below 75 μm. The chemical composition of the glass powder presented in Table 1 was determined by X-ray fluorescence analysis using a wavelength dispersive spectrometer (S8 Tiger, Bruker, Billerica, MA, USA).

The glass powder was activated by casting it in 2.5 M CsOH aqueous solution, prepared by dispersing reagent-grade CsOH powder (Sigma - Aldrich, Darmstadt, Germany) in deionized water. The solid loading was set at 60 wt %. The glass suspension was mechanically stirred at 500 rpm for 150 min to ensure partial dissolution and uniform dispersion of glass particles in the alkaline solution. The suspension was poured into polystyrene moulds and covered with a perforated polyethylene film, allowing for slow and controlled condensation and dehydration reactions. The moulds were placed in an oven at 40 °C and left to cure for 7 days. Twelve dried specimens, each measuring approximately 10 mm × 10 mm x 7 mm (length x width x height), were carefully removed from the mould and analyzed; some pieces were put in boiling deionized water for 15 min and then dried at 75 °C for 3 h. The samples from direct alkali activation and those subjected to boiling treatment after the activation were labelled as BASG-a and BASG-b.

The dimensions of alkali-activated cubes were measured with a digital calliper. The surface area of each sample was calculated based on the measured dimensions and the geometric shape. Dried samples were sintered in air at 700 °C, at a heating rate of 10 °C/min and a dwelling time of 1 h. To determine the mass loss of BASG-a during sintering, a sample fragment was analyzed using differential thermal analysis-thermogravimetric analysis (DTA/TG, TA Instruments® SDT-Q600, New Castle, USA) with the same experimental settings as the sintering process.

The bulk density of the alkali-activated and sintered samples was measured by considering their mass measured with an analytical balance and their volume. Helium pycnometry (Ultrapyc 3000, Anton Paar GmbH) was used to determine the apparent and true density of the samples. The porosity was calculated using the values obtained from the measurements. The results represent the average values of 3–5 individual tests.

To evaluate the aqueous corrosion resistance, leaching tests were performed on sintered BASG-a and BASG-b samples using the Materials Characterization Center-1 Standard (MCC-1: ASTM C1220-10) (ASTM International, 2021). The samples were placed in Teflon containers with deionized water, with a surface area to water volume ratio (S/V) of 10 m^{-1}. The leaching experiments were conducted under static conditions at 90 °C. After 7 days, the samples were removed from the containers and weighed with an analytical balance with a precision of $1{\cdot}10^{-4}$ g. An aliquot of the leachate was analyzed by inductively coupled plasma-mass spectrometry (Spectro Genesis ICP-MS 7900 Agilent, Santa Clara, USA). The normalized leaching rate NLR (g/m^2d) was determined from the chemical analysis of the leachant.

All samples were examined by scanning electron microscopy (FEI, Quanta 200 ESEM, Eindhoven, The Netherlands), energy dispersive spectroscopy (EDS/EDAX Genesis, Mahwah, NJ, USA), and Fourier transform infrared spectroscopy (FTIR Jasco 4200, Jasco, Japan). The surfaces of the samples for SEM analysis were sputter coated with platinum. FTIR spectra were measured in absorbance mode on a powder with a particle size below 75 μm, covering the spectral range from 4000 to 400 cm^{-1}. X-ray powder diffraction analyses were performed using a D8 Advance machine (Bruker AXS, Karlsruhe, Germany) operating at 40 kV and 40 mA with CuKα radiation (0.15418 nm) in the 2θ range from 9 to 70°, with a step size of 0.02° and counting time of 2 s per step. Phase identification was performed using the HighScore Plus V. 3.0 d software, (PANanalytical B.V., Almelo, The Netherlands) with the COD2023 database. Structural refinement was performed on a BASG-b diffraction pattern using HighScore Plus 4 program packages (PANanalytical B.V., Almelo, The Netherlands) based on the Rietveld method, (Rietveld, 1969).

Table 1
Chemical composition of the received boro-alumino-silicate glass.

Chemical analysis (wt. %)						
SiO_2	B_2O_3	Na_2O	Al_2O_3	CaO	K_2O	BaO
74 ± 2	9.6 ± 2	7 ± 0.5	6.6 ± 0.2	1.1 ± 0.2	1.08 ± 0.06	0.62 ± 0.07

3. Results and discussion

The activating solution was prepared from non-radioactive CsOH; this compound, however, is recognized as chemically identical to its radioactive counterpart based on the 'critical' ^{137}Cs isotope (Kamei-Ishikawa et al., 2008). After drying, the activated glass suspension formed crack-free bodies (Fig. 3a) that did not degrade even after immersion in boiling deionized water for 15 min, in analogy with bodies from NaOH/KOH or NaOH activation, (Mehta et al., 2022; Lago et al., 2023).

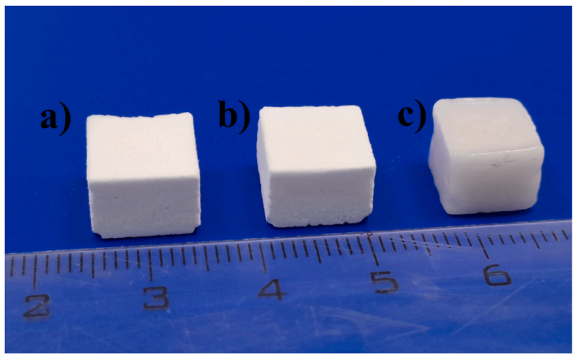

Fig. 3. a) Appearance of alkali-activated glass after CsOH attack and hardening, b) after immersion in boiling water, and c) after sintering at 700 °C and leaching.

Dissolution of glass particles and the subsequent condensation can be achieved by adjusting the pH value of the alkali activator. This process is favoured at a pH level of 11 or higher. Although it can still occur at lower pH values, the activation process is a delayed reaction (Fernández-Jiménez and Puertas, 2003). In analogy with recent studies, concerning alkaline attack at low molarity (Tameni et al., 2022), a diluted CsOH solution (2.5 M, pH 13) was used.

Previous research demonstrated that the activation of BASG with NaOH/KOH or NaOH (Tameni et al., 2022; Lago et al., 2023; Mehta et al., 2022, yielded upon drying a stable cementitious matrix. As discussed in the introduction, after partial dissolution hydrated layer forms on the surface of glass particles. Condensation reactions, such as the reconstruction of Si–O–Si bridges from silanols (Si–OH) from two adjacent glass particles proceed in the hydrated layers (Fig. 2), similar to weathering of nuclear glass (Majérus et al., 2020). Alkalis from the activating solution react with the products of dissolution and/or the atmosphere, generating secondary phases. These include crystalline hydrated alkali carbonates that can be eliminated by boiling the samples in water.

The FTIR results confirmed the evolution of suspensions of BASG, as seen in the transition from NaOH or NaOH/KOH to CsOH activation. When comparing the FTIR spectra of the as received glass and the activated material, both dried and after boiling, only minimal changes were observed (Fig. 4a). The bands attributed to Si–O (Si) and Si–O (Al) stretching (at approximately 1010 cm^{-1}) and Si–OH bending (880 cm^{-1}) vibrations showed no significant displacement or reduction in intensity, except for the Si–O stretching peak, which shifted from 1010 cm^{-1} to 990 cm^{-1} as a result of formation of the hydrated gel (Lancellotti et al., 2013).

A weak band attributed to C–O stretching vibration detected at around 1405 cm^{-1} after activation and almost disappearing after boiling, is consistent with the formation of carbonates resulting from the reactions with CO_2 absorbed from the atmosphere (García-Lodeiro et al., 2010). After activation, and to a lesser extent also after boiling treatment, a vibration associated with the presence of OH^- groups and zeolitic water in the structure was observed at 1634 cm^{-1} (Omeragević et al., 2016). The bands between 600 and 800 cm^{-1} correspond to Al–O–Si stretching vibrations while the Al(IV)–O stretching vibrations are found around 790 cm^{-1}, (Lancellotti et al., 2013).

Some signals are attributable to important transformations induced by CsOH activation. The shoulder of the main band, located at 880-900 cm^{-1}, is likely associated with the stretching of a boron-oxygen bond in tetragonal configuration (Mehta et al., 2022). The signal, found after activation was preserved also after boiling. On the contrary, the intensity of the band at about 1405 cm^{-1} increased after the activation but it returned to its initial value after boiling. A preliminary interpretation of the first, 'permanent' extra band, is a change in the balance between BO_3 and BO_4 units (the latter stabilized by alkali in the surrounding spaces) typically found in borosilicate glasses (Mehta et al., 2022). The second additional band is attributed to the stretching vibration of the C–O bond present in hydrated carbonates (as previously found in glasses activated in NaOH/KOH solutions), which dissolved upon boiling (Garcia-Lodeiro et al., 2014).

X-ray powder diffraction analysis (Fig. 4b) provided a significant contribution to the understanding of the extra signals in FTIR spectra. Weak diffraction maxima in the pattern of the activated material are consistent with the formation of hydrated cesium carbonate ($CsHCO_3$, PDF #01-084-2364). More pronounced diffraction lines appearing in the activated material and remaining after boiling are of particular interest, since they match closely (with the exception of a slight shift at higher 2θ values) the diffraction pattern of boro-pollucite ($Cs_{0.814}B_{1.092}(Si_{1.977}O_6)$; PDF #98-041-3224). The formation of an anhydrous phase is unprecedented and finds analogies only with the evolution of geopolymer-yielding slurries, activated under more complex conditions (e.g., extensive alkaline attack) (Arbel-Haddad et al., 2023).

Crystalline alkali boro-silicates represent structural analogies with alkali alumino-silicates (Bubnova et al., 2004). In particular, feldspars (alumino-silicates) may be considered 'stuffed derivatives' of crystalline silica variants, with SiO_4 units replaced by AlO_4 units balanced by alkali

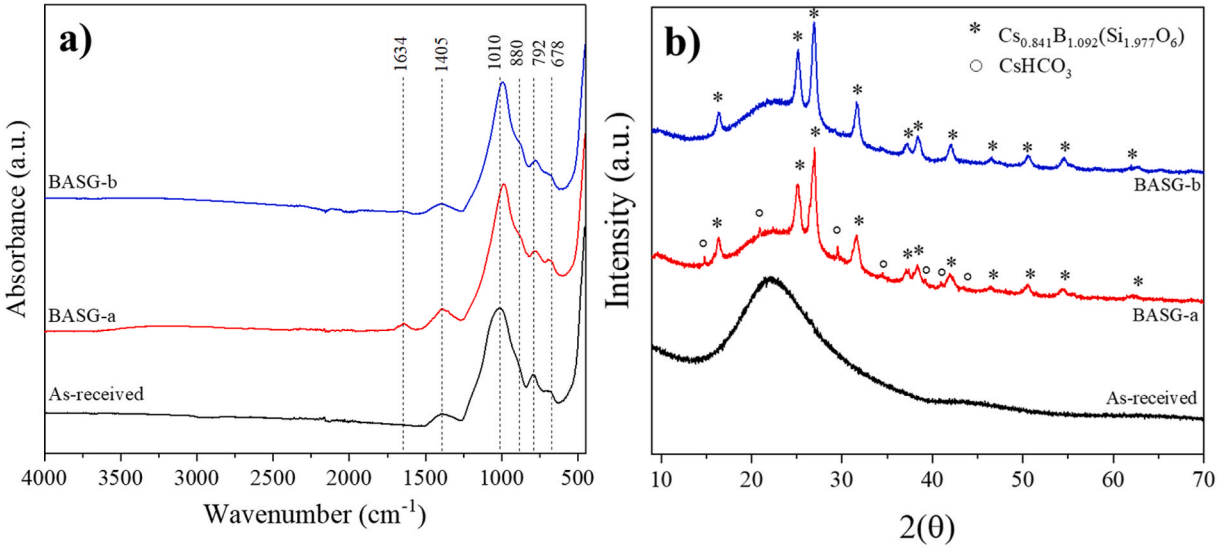

Fig. 4. a) FTIR spectra and b) X-ray diffraction patterns of the as-received glass, alkali-activated (BASG-a) and boiled (BASG-b).

ions. Boro-pollucite features an analogous replacement of SiO_4 units with BO_4 units. In other words, the observed 'extra band' in FTIR could be attributed to a newly formed insoluble phase, instead of any change in the glass structure.

Unlike the activation with NaOH/KOH where boiling treatment acted as an 'etching' of the newly formed soluble (amorphous and crystalline) phases, the CsOH-activated sample was not completely affected by the boiling treatment (Fig. 4b). According to the diffractogram of BASG-b, the carbonate phase disappeared, whereas boro-pollucite stayed intact. The immersion in boiling water did not disintegrate the samples (Fig. 3b).

Table 2 shows the chemical composition of the alkali-activated glass before and after boiling, determined by EDS. The results prove that cesium remained in the sample even after boiling.

Cross sections of the samples were analyzed by SEM-EDS. Fig. 5 shows SEM micrographs of the alkali-activated surfaces after 7 days of curing at 40 °C before (Fig. 5 a-c) and after (Fig. 5 d-f) boiling test. The chemical composition of selected sites was assessed by energy-dispersive spectroscopy (EDS, spectra shown in Fig. 5c and f).

Cs-containing phases had a quite distinctive morphology. Fig. 5a–b illustrate the presence of fibrous crystals, in which high concentrations of cesium can be confirmed by the detection of back-scattered electrons. Heavier elements are known to appear brighter than lighter materials; this effect, although less pronounced, is also found in secondary electron images (Goldstein et al., 2018). The results of EDS analysis in Fig. 5c reveals a high concentration of cesium (~55 wt %) and a substantial amount of carbon. This suggests that the phase can be associated with (hydrated) cesium carbonate.

The association of fibrous crystals with cesium carbonate was confirmed by the analysis of samples after boiling (Fig. 5d–e). Due to their solubility, the fibrous crystals disappeared during boiling (the solubility of cesium carbonate is 209 g/100 g H_2O, at 20 °C (Green, M., & Southard, 2019)), and were no longer present. However, cesium was not removed completely: lightly coloured areas (Fig. 5e) could be attributed to gel embedding boro-pollucite crystals. A high concentration of cesium is confirmed by the EDS spectrum (Fig. 5f), also confirming a significant content of aluminium.

A first hypothesis involved the inclusion of aluminium in a boro-pollucite solid solution, described by the formula $Cs(Al_xB_{1-x})Si_2O_6$ with pure pollucite and pure boro-pollucite as the end members. The degree of substitution of B^{3+} ions with Al^{3+} (x value) should actually be quite low. As mentioned above, the experimental positions of diffraction maxima in XRD patterns did not exactly match the theoretical pattern of boro-pollucite (PDF #98-041-3224) (Figs. 4b and 6 (blue solid lines)). However, the theoretical pattern could be used as a starting model for Rietveld refinement.

A good fit (Fig. 6, red solid lines) was obtained by refining cell parameters, profile parameters, background and a single broad peak for the glass hump, atomic positions, site occupancy factors (s.o.f.) and thermal parameters (Biso). The refined cell parameters were a = 13.2499(6) and V = 2326.1 (1). Table 3 contains the additional refined structural parameters. The refinement conditions indicate that a boro-pollucite variant, like $Cs_{0.814}B_{1.092}(Si_{1.977}O_6)$ (PDF #99-001-0001), offers a superior match of the experimental pattern. In other words, the 2θ-shifts can be attributed simply to the B/Si balance, rather than to the substitution of B with Al. Aluminium, as a consequence, was likely present only in the gel surrounding boro-pollucite crystals.

Table 2
Chemical composition of alkali-activated BASG samples before and after boiling.

Sample	Chemical analysis (wt. %)							
	O	Si	Na	Al	K	C	Ca	Cs
BASG-a	38.8 ± 4	18.9 ± 3	3.7 ± 0.4	1.9 ± 0.1	0.3 ± 0.04	9.2 ± 1	0.6 ± 0.03	26.5 ± 3
BASG-b	48 ± 7	25.1 ± 2	3.9 ± 0.1	2.5 ± 0.1	0.4 ± 0.05	7.1 ± 2	0.7 ± 0.02	12.3 ± 4

The boiling treatment removed part of the material present between packed glass particles. The results of pycnometric measurements presented in the Table 4 supported this assumption, showing simultaneous increase of overall and open porosity after boiling. Both before and after boiling the porosity was almost exclusively open.

The low temperatures required to trap and retain cesium represent one of the most important findings of the present investigation. The bodies synthesized through the cold consolidation with CsOH, whether dried or boiled, can be further treated by viscous flow sintering to further stabilize the immobilized cesium. This process aims to create solid waste-forms with limited (closed) residual porosity. For glass, the optimum temperature for pressure-less sintering is approximately 50 °C higher than the dilatometric softening temperature (Ray and Tiwari, 2001). In our previous works the dilatometric sintering temperature of BASG was determined to be about 650 °C (Mehta et al., 2022). In this study, the alkali-activated samples were non-isothermally sintered in air at 700 °C at a heating rate of 10 °C/min and 1 h dwelling time. To assess the potential volatilization of cesium during sintering, a DTA-TG analysis of the BASG-a sample was performed under identical conditions to those of the sintering process. The thermal behaviour and mass change during the heating of BASG-a sample from 25 to 800 °C are presented in Fig. 7.

As the temperature of the heat treatment increases, a gradual increase mass loss is observed. The TG curve shows a final mass loss of 3.2 %, which is attributed to the loss of water. This is confirmed by the DTA curve, which shows a weak endothermic peak at 220 °C. Approximately one third of the mass loss of the sample is observed below 200 °C, which is associated with dehydration and release of molecules of physisorbed water (Sotelo-Piña et al., 2019). The remaining mass loss takes place in the range of 200–700 °C and is attributed to the loss of structural water and dehydration of superficial silanol groups, (He et al., 2016), along with decomposition of carbonates. It is important to mention that significant cesium volatilization is not expected during the thermal treatment at 700 °C. He et al. reported that cesium evaporation is expected only during thermal treatments at the temperatures higher than 1090 °C (He et al., 2016). The sintering temperature used here is almost 300 °C lower than the temperature used to synthetize zeolites. The thermogravimetric analysis confirms that the mass loss is almost negligible in the studied temperature range.

BASG-a and BASG-b samples were almost completely densified after sintering at 700 °C. As reported in Table 5, the overall porosity was reduced by 21 and 25 %. The firing also resulted in an abundant shrinkage, ranging from 18.3 ± 4 % to 19.5 ± 3 %, for BASG-a and BASG-b samples, respectively.

The decrease of the residual porosity is illustrated also by the change of morphology. In BASG-a (dried) a more abundant release of volatile moieties resulted in the formation of closed pores (Fig. 8 a-b) with a diameter ranging from 2 to 20 μm. Sintered BASG-b features more isolated pores with diameters ranging approximately between 2 and 40 μm. Back-scattered electron images (Fig. 8b and e in particular) reveal a more uniform distribution of cesium, which is lower in darker areas observed in BASG-b (see Fig. 8c and f). The EDS analysis (of the whole areas shown in Fig. 8b and e confirmed that the average cesium content in both samples is almost the same as before sintering: ~25 wt % in BASG-a sample and 12 wt % in the BASG-b sample.

Open pores and interconnected porosity have direct implications on the functionality of the alkali-activated glass as a waste-form for long-term storage and final disposal of nuclear waste. Upon accidental contact with water, a lower open porosity implies a smaller contact surface between the host matrix and the aqueous medium and therefore a lower probability of leaching of immobilized cesium.

X-ray diffraction patterns of both fired samples are shown in Fig. 9. The pattern of BASG-b sample is also added for comparison. Traces of

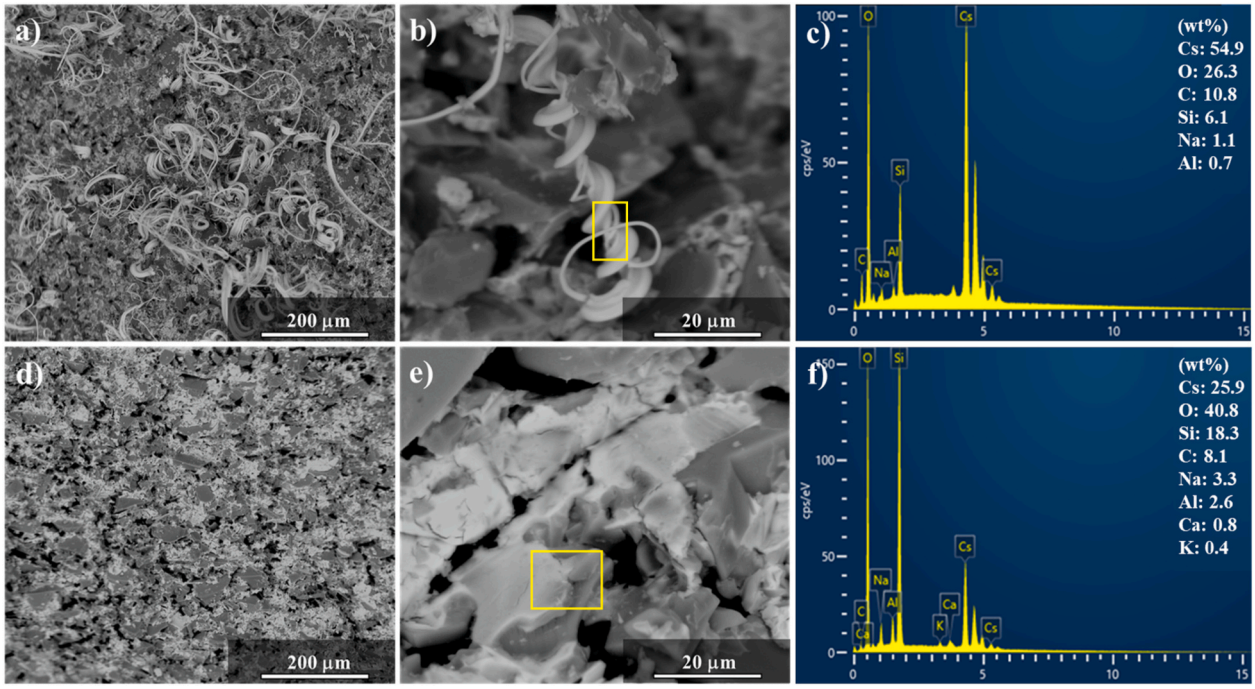

Fig. 5. SEM micrograph on a-c) BASG-a and d-f) BASG-b and EDS analyses on respective sites.

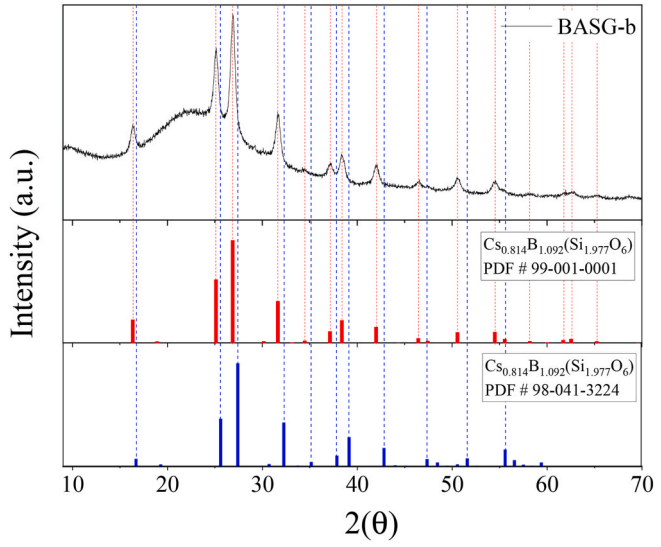

Fig. 6. X-ray diffractogram of the alkali-activated and boiled sample (BASG-b) compared with reference pattern of boro-pollucite before (PDF #98-041-3224) and after (PDF #99-001-0001) Rietveld refinement.

Table 3
Detail of atomic positions and occupancies of the boro-pollucite crystal phase.

Atom	Wyckoff	S.O.F.	X	Y	Z	Biso
B1	48 g	0.20(9)	0.1(1)	0.66(7)	0.59(7)	2(1)
O1	96 h	1.000000	0.0288(7)	0.1159(5)	0.3509(6)	1(1)
Si1	48 g	0.80(9)	0.1(1)	0.66(7)	0.59(7)	2(1)
Cs1	16 b	1.00(3)	0.125000	0.125000	0.125000	3.48(8)

Table 4
Density and porosity of BASG-a and BASG-b samples after alkaline activation and boiling.

Sample	Density (g/cm^3)			Porosity (%)		
	Geometric	Apparent	True	Total	Open	Closed
BASG-a	1.84 ± 0.5	2.47 ± 0.5	2.51 ± 0.3	26.7 ± 0.7	25.5 ± 0.6	1.3 ± 0.1
BASG-b	1.67 ± 0.5	2.46 ± 0.6	2.5 ± 0.2	33.2 ± 0.5	32.1 ± 0.5	1.1 ± 0.1

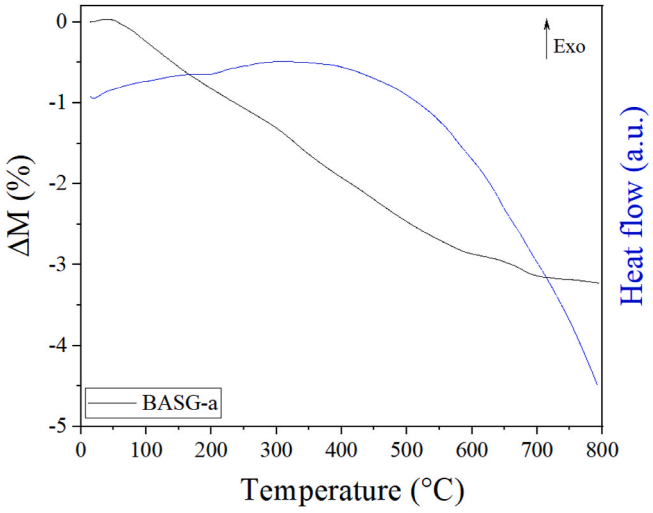

Fig. 7. DTA-TG measurements of BASG-a sample.

boro-pollucite were preserved after firing of BASG-b, featuring the highest cesium content. The softening of glass resulted in an almost complete dissolution of the crystalline phase, as indicated by the absence of colour gradients in the light-grey zones (which could occur in the presence of interfaces between crystals and glass matrix) in Fig. 8 a-b and Fig. 8 d-e.

During the final disposal of immobilized waste, the contact between waste-form and groundwater is the most likely mechanism by which radionuclides may be released from the waste-form (Zhen-Wu et al.,

Table 5
Density and porosity of BASG-a and BASG-b samples after sintering.

Sample	Density (g/cm^3)			Porosity (%)		
	Geometric	Apparent	True	Total	Open	Closed
BASG-a, 700	2.34 ± 0.2	2.27 ± 0.3	2.5 ± 0.1	5.64 ± 0.3	–	5.64 ± 0.3
BASG-b, 700	2.28 ± 0.3	2.40 ± 0.4	2.47 ± 0.3	7.7 ± 0.4	5 ± 0.2	2.7 ± 0.2

2021). The efficiency of the waste immobilization process is thus measured in terms of the resistance of the sintered material to aqueous corrosion. After the leaching tests, the sintered samples were taken out of the Teflon containers. The samples appeared to be well-consolidated bodies and did not experience any shelling or cracks as a result of the corrosion test (Fig. 3c). No change in the mass of the dried BASG-a and BASG-b samples heat treated at 700 °C after their removal from the aqueous media was observed.

Different aliquots corresponding to the BASG-a,700 and BASG-b,700 samples were taken from the leaching solutions and analyzed in duplicate using ICP-MS. This technique is very sensitive, having a detection limit for cesium of 0.482 μg/L (ppb Cs). The cesium concentration in all solutions was below the detection limit of the technique, which indicates a cesium leaching rate at the order of $1{\cdot}10^{-4}$ g/m^{2}d. This value is approximately one order of magnitude lower than that obtained by Feng et al. from a synthesis with silica gel using a type of zeolite-4A under analogous experimental conditions (Feng et al., 2023). This result is also in agreement with the work carried out with geopolymer consolidated at higher temperatures (≤1000 °C) by He et al. who obtained a similar leaching rate ($2.5{\cdot}10^{-4}$ g/m^{2}d), (He et al., 2019). Cesium stabilization thus benefits from the high chemical durability of pharmaceutical boro-alumino-silicate glass.

A summary of the evolution of CsOH-activated glass (based on FTIR, XRD and EDS-SEM findings) is presented in Fig. 10.

The bonding of particles is still attributed to condensation of Si–OH, B–OH, and Al–OH terminals at the surface of adjacent particles. Dissolution products and the atmosphere contribute to the development of multiple secondary phases, with distinctive elemental distribution. Aluminium ions, absent in boro-pollucite solid solution ($Cs_{0.82}B_{1.09}Si_{1.98}O_6$), contribute to the formation of a stable amorphous gel (i.e. resisting to boiling). The only 'weakness' concerns the formation of soluble cesium carbonate: future investigations will undoubtedly involve the reduction or elimination of this phase, to realize a complete immobilization of cesium at nearly room temperature, e.g. by enhancing the release of glass components into the solution without altering the overall cesium content (CsOH possibly coupled with organic bases).

In a glass suspensions hardened without boiling, the activation can be seen as a preliminary step before sintering at relatively low temperature (700 °C). Table 6 presents the comparison with other waste forms that included sintering as the final step for cesium immobilization.

It should be noted that although there are studies that allow a higher percentage of cesium to be retained, the experimental conditions used are more demanding, since they require higher temperatures (Feng et al., 2023; He et al., 2019; J. H. Yang et al., 2017), longer treatment times (Feng et al., 2023; Jing et al., 2016; J. Liu et al., 2021), or the use of unconventional sintering methods (Omeragević et al., 2016; Xiang et al., 2021).

Another crucial aspect to consider is not only the percentage of cesium retained in the host matrix but also the percentage that effectively remains embedded in the matrix after leaching tests. The analysis of Table 6 reveals that there are studies where the percentage of immobilized cesium is comparable (or even better) to that retained in this work, but their leaching rates are higher under similar leaching conditions (Fu et al., 2020; Omeragević et al., 2016; Yang et al., 2020).

Various methodologies have been developed for retaining an ion with physicochemical properties as complex as those of cesium. Selecting a specific method requires meticulous analysis to strike a balance between the actual amount of cesium retained and the associated economic and environmental costs. The method developed in this study offers optimal storage conditions for a significant percentage of

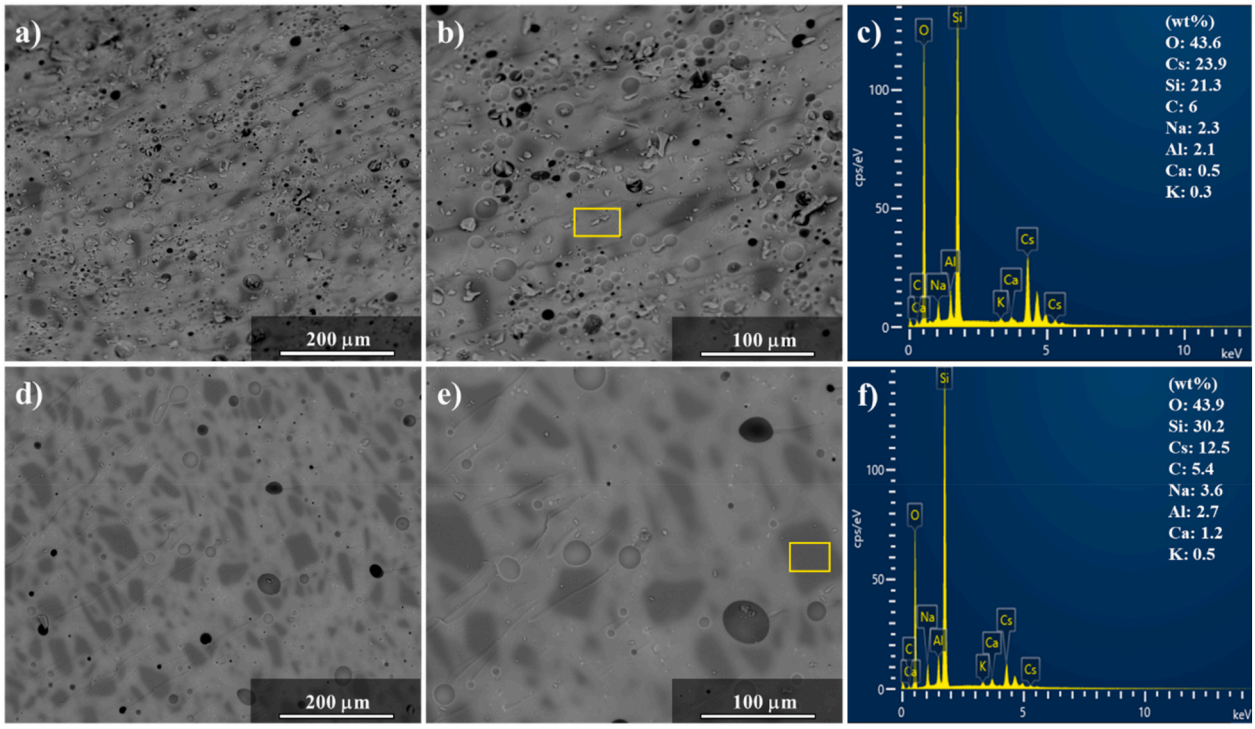

Fig. 8. SEM micrographs of the cross-sections of alkali-activated glass: a-c) BASG-a and d-f) BASG-b, after sintering at 700 °C-1h. Figures (c) and (f) respectively show the EDS spectra of the areas outlined by yellow rectangles. (For interpretation of the references to colour in this figure legend, the reader is referred to the Web version of this article.)

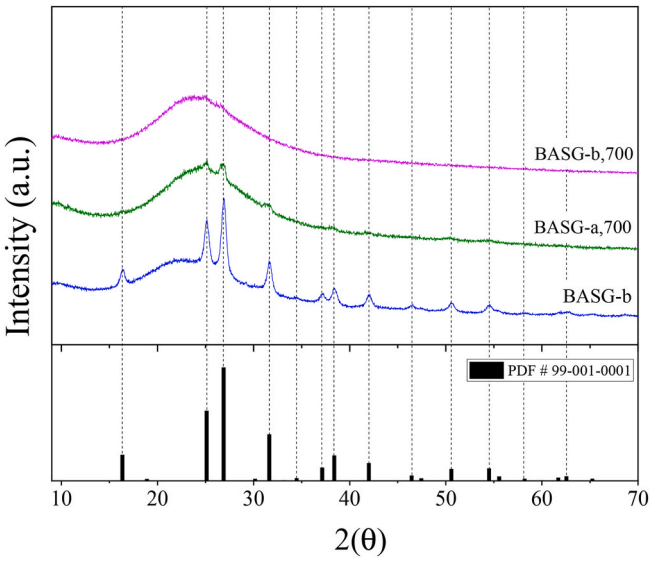

Fig. 9. X-ray diffractograms of BASG-a (green line) and BASG-b (magenta line) samples after sintering (700 °C-1h) compared with the reference pattern for boro-pollucite $Cs_{0.814}B_{1.092}(Si_{1.977}O_6)$, (PDF #99-001-0001). The diffractogram of BASG-b sample before firing was also added for comparison (blue line). (For interpretation of the references to colour in this figure legend, the reader is referred to the Web version of this article.)

cesium. Notably, our approach adheres to sustainability principles, utilizing discarded pharmaceutical glass vials and a diluted CsOH solution as the activating medium.

4. Conclusions

Immobilization of over 20 wt % cesium was achieved through alkaline activation of a pharmaceutical boro-alumino-silicate glass and a cold consolidation process. The main novelty lies in a very low temperature used to immobilize cesium, partially incorporated in a framework mineral structure of boro-pollucite, which has been recognized as one of the most promising options for the storage of radioactive cesium.

At least for the part stored in boro-pollucite, cesium is immobilized already after cold consolidation, leading to blocks withstanding immersion in boiling water. After alkali activation the used boro-alumino-silicate glass from pharmaceutical vials yielded a cementitious matrix formed by condensation reactions at the surface of attacked glass particles. Boro-pollucite represents the first example of an insoluble crystalline phase that is formed through the combination of activation by an alkaline compound (CsOH) and glass dissolution products.

Further stabilization was achieved through the use of glass matrix, which was viscous flow sintered at the temperature as low as 700 °C. The content of cesium remained almost constant before and after sintering, in both cold consolidated and boiled samples. The leaching test showed that the release of cesium was very low (lower than 0.482 ppb), regardless of its concentration in sintered samples.

CRediT authorship contribution statement

Diana Lago: Writing – review & editing, Writing – original draft, Methodology, Investigation, Formal analysis, Data curation, Conceptualization. **Giulia Tameni:** Writing – original draft, Methodology, Investigation, Data curation. **Federico Zorzi:** Formal analysis, Data curation. **Jozef Kraxner:** Writing – review & editing, Visualization, Supervision, Funding acquisition. **Dušan Galusek:** Writing – review & editing, Supervision, Project administration, Funding acquisition. **Enrico Bernardo:** Writing – review & editing, Visualization, Supervision, Resources, Methodology, Funding acquisition, Data curation, Conceptualization.

Declaration of competing interest

The authors declare the following financial interests/personal relationships which may be considered as potential competing interests:

Dusan Galusek reports financial support was provided by H2020 research and innovation programme (g.a. 739566). Enrico Bernardo reports financial support was provided by MUR PON R&I 2014–2021. If there are other authors, they declare that they have no known competing financial interests or personal relationships that could have appeared to influence the work reported in this paper.

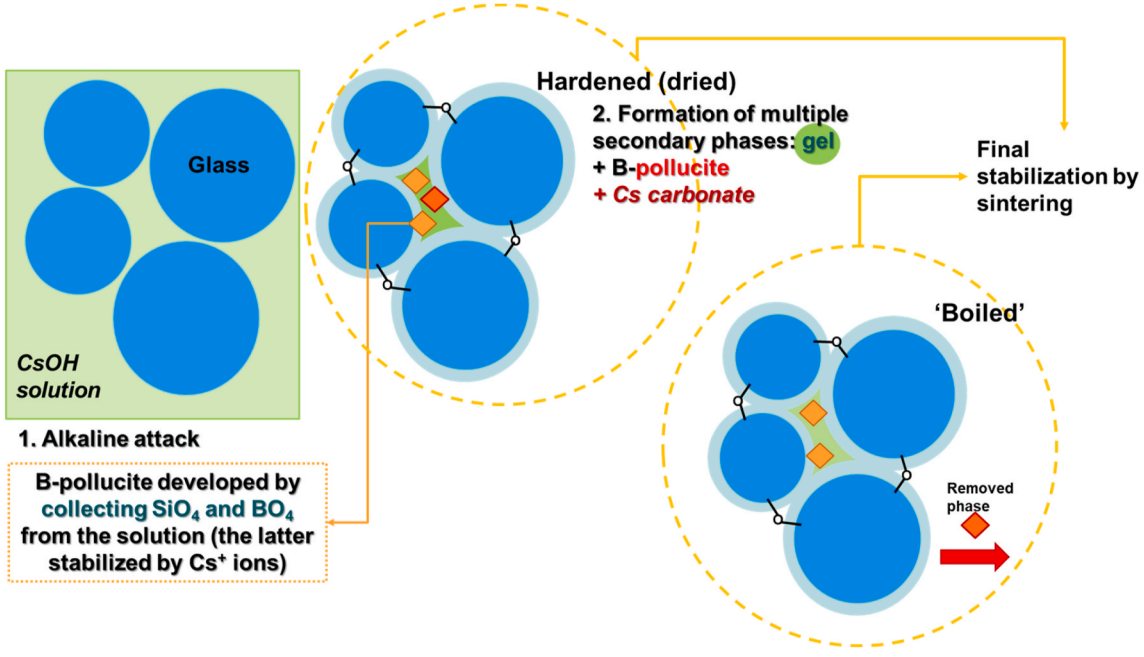

Fig. 10. Schemes of alkali activation and cold consolidation from CsOH solution.

Table 6
Cesium waste forms and leaching values reported in other works.

Precursors	Method	Waste form	Cs retain (wt %)	Leaching rate (g/m^2·d)	Ref
Silica-based ammonium molybdophosphate (AMP/SiO_2)	Adsorption + sintering (1200 °C, 1 h)	AMP-Cs/SiO_2	2.1	$9{\cdot}10^{-5}$	Wu et al. (2018)
Blast furnace slag/NaOH	Alkali-activation + 95 °C, 24 h	AABFS	2–5	$6{\cdot}10^{-3}$	Komljenović et al. (2020)
Metakaolin geopolymer-zeolite	Sintering (1100 °C, 6 h)	Cs-pollucite	4.5	$5{\cdot}10^{-3}$	Li et al. (2022)
Rice husk ash/CsOH, $Ca(OH)_2$	Hydrothermal (200 °C, 10 h, 30 MPa)	Pollucite	6	$2.31{\cdot}10^{-5}$	Jing et al. (2016)
Metakaolin-CsOH, NaOH	Hydrothermal (200 °C, up to 30 h, 30 MPa)	Analcime/Pollucite	6.2	$4.3{\cdot}10^{-6}$	Liu et al. (2021)
Cs-LTA zeolite	Adsorption + hot-pressing (750 °C, 3 h, 35 MPa)	Pollucite	24	$9.3{\cdot}10^{-2}$	Omerašević et al. (2016)
Cs/metakaolin/glass	Sintering (1050 °C, 2 h)	Geopolymer	25	$4{\cdot}10^{-3}$	Yang et al. (2020)
Glass frit/Cs-filter	Melting (1000 °C, 3 h)	Pollucite	30	$7.2{\cdot}10^{-5}$	Yang et al. (2017)
Metakaolin-based geopolymer	Microwave sintering (1200 °C, 0.5 h)	Pollucite	30	$3{\cdot}10^{-4}$	Xiang et al. (2021)
Metakaolin-based geopolymer	Hydrothermal (200 °C, 6 h)	Pollucite	31	$1.1{\cdot}10^{-2}$	Fu et al. (2020)
Na,Cs-geopolymer	Sintering (1000 °C, 2 h)	Geopolymer	33	$2.5{\cdot}10^{-4}$	He et al. (2019)
CsOH-Zeolite-4A	Sintering (900 °C)	Pollucite	36	$1{\cdot}10^{-3}$	Feng et al. (2023)
BASG/CsOH	Alkali-activation + sintering (700 °C, 1 h)	Boro-pollucite	20	$<1{\cdot}10^{-4}$	**This work**

Data availability

Data will be made available on request.

Acknowledgements

This paper is a part of the dissemination activities of the FunGlass project. This project has received funding from the European Union's Horizon 2020 research and innovation programme under grant agreement No. 739566. The authors also gratefully acknowledge the financial support from the Slovak Grant Agency of the Ministry of Education, Science, Research and Sport, VEGA No 1/0456/20. Publication was created also in the frame of project: Advancement and support of R&D for Centre for diagnostics and quality testing of materials in the domains of the RIS3 SK specialization, ITMS2014+:313011W442, based on the Operational Programme Integrated Infrastructure and funded from the European Regional Development Fund. G.T. and E.B. acknowledge the support of national project MUR PON R&I 2014–2021. Dr. Hana Kaňková and Dr. Silvia Zanatta are gratefully acknowledged for the ICP-MS and DTA-TG analysis.

References

Arbel-Haddad, M., Ofer-Rozovsky, E., Goldbourt, A., 2023. Facile formation of pollucite in geopolymers: implications for radioactive Cs immobilization. Ceram. Int. 49 (18), 30881–30885. https://doi.org/10.1016/j.ceramint.2023.07.006.

ASTM International, 2021. Test Method for Static Leaching of Monolithic Waste Forms for Disposal of Radioactive Waste. ASTM International, West Conshohocken, PA, USA. https://doi.org/10.1520/C1220-21.

Bosch, P., Caputo, D., Liguori, B., Colella, C., 2004. Safe trapping of Cs in heat-treated zeolite matrices. J. Nucl. Mater. 324 (2–3), 183–188. https://doi.org/10.1016/j.jnucmat.2003.10.001.

Bubnova, R.S., Stepanov, N.K., Levin, A.A., Filatov, S.K., Paufler, P., Meyer, D.C., 2004. Crystal structure and thermal behaviour of boropollucite $CsBSi_2O_6$. Solid State Sci. 6 (7), 629–637. https://doi.org/10.1016/j.solidstatesciences.2004.03.015.

Caurant, D., Loiseau, P., Majerus, O., Aubin-Chevaldonnet, V., Bardez, I., Quintas, A., 2007. Glasses, glass-ceramics and ceramics for immobilization of highly radioactive nuclear wastes. In: Caurant, D. (Ed.), Glasses, Glass-Ceramics and Ceramics. Hauppauge: Nova Science Publishers, Inc., France, pp. 2–20.

Davidovits, J., 2011. Geopolymer Chemistry and Applications, fourth ed. Institut Géopolymére, Saint-Quentin, France.

El-Eswed, B.I., 2020. Chemical evaluation of immobilization of wastes containing Pb, Cd, Cu and Zn in alkali-activated materials: a critical review. J. Environ. Chem. Eng. 8 (5), 104194 https://doi.org/10.1016/j.jece.2020.104194.

Feng, Y., Wei, G., Liu, Y., Zhang, Z., Yan, M., He, X., Miao, Y., Yuan, B., Zhang, Y., Ban, Z., Song, Z., Lu, X., 2023. Synthesis and characterization of pollucite: a low-temperature immobilization method for ^{137}Cs. J. Radioanal. Nucl. Chem. 332 (2), 467–478. https://doi.org/10.1007/s10967-022-08736-w.

Fernández-Jiménez, A., Puertas, F., 2003. Effect of activator mix on the hydration and strength behaviour of alkali-activated slag cements. Adv. Cement Res. 15 (3), 129–136. https://doi.org/10.1680/adcr.2003.15.3.129.

Fu, S., He, P., Wang, M., Cui, J., Wang, M., Duan, X., Yang, Z., Jia, D., Zhou, Y., 2020. Hydrothermal synthesis of pollucite from metakaolin-based geopolymer for hazardous wastes storage. J. Clean. Prod. 248, 119240 https://doi.org/10.1016/j.jclepro.2019.119240.

García Lodeiro, I., Fernández-Jimenez, A., Palomo, A., Macphee, D.E., 2010. Effect on fresh C-S-H gels of the simultaneous addition of alkali and aluminium. Cement Concr. Res. 40 (1), 27–32. https://doi.org/10.1016/j.cemconres.2009.08.004.

Garcia-Lodeiro, I., Fernández-Jimenez, A., Pena, P., Palomo, A., 2014. Alkaline activation of synthetic aluminosilicate glass. Ceram. Int. 40 (4), 5547–5558. https://doi.org/10.1016/j.ceramint.2013.10.146.

Gatta, G.D., Rotiroti, N., Zanazzi, P.F., Rieder, M., Drabek, M., Weiss, Z., Klaska, R., 2008. Synthesis and crystal structure of the feldspathoid $CsAlSiO_4$: an open-framework silicate and potential nuclear waste disposal phase. Am. Mineral. 93 (7), 988–995. https://doi.org/10.2138/am.2008.2729.

Goldstein, J.I., Newbury, D.E., Michael, J.R., Ritchie, N.W.M., Scott, J.H.J., Joy, D.C., 2018. Scanning Electron Microscopy and X-Ray Microanalysis, 4 ed. Springer International Publishing, New York, NY. https://doi.org/10.1007/978-1-4939-6676-9.

Green, M., Southard, D., 2019. Perry's Chemical Engineers' Handbook, ninth ed. Mc Graw Hill Education, New York, United States.

He, P., Wang, M., Fu, S., Jia, D., Yan, S., Yuan, J., Xu, J., Wang, P., Zhou, Y., 2016. Effects of Si/Al ratio on the structure and properties of metakaolin based geopolymer. Ceram. Int. 42 (13), 14416–14422. https://doi.org/10.1016/j.ceramint.2016.06.033.

He, P., Wang, R., Fu, S., Wang, M., Cai, D., Ma, G., Wang, M., Yuan, J., Yang, Z., Duan, X., Wang, Y., Jia, D., Zhou, Y., 2019. Safe trapping of cesium into doping-enhanced pollucite structure by geopolymer precursor technique. J. Hazard Mater. 367, 577–588. https://doi.org/10.1016/j.jhazmat.2019.01.013.

Hunter, D.B., Salzman, J.E., Zaelke, D., 2022. Glasgow climate summit: cop26. SSRN Electron. J. 1–12. https://doi.org/10.2139/ssrn.4005648.

Idir, R., Cyr, M., Pavoine, A., 2020. Investigations on the durability of alkali-activated recycled glass. Construct. Build. Mater. 236, 117477 https://doi.org/10.1016/j.conbuildmat.2019.117477.

Jing, Z., Hao, W., He, X., Fan, J., Zhang, Y., Miao, J., Jin, F., 2016. A novel hydrothermal method to convert incineration ash into pollucite for the immobilization of a simulant radioactive cesium. J. Hazard Mater. 306, 220–229. https://doi.org/10.1016/j.jhazmat.2015.12.024.

Kamei-Ishikawa, N., Tagami, K., Uchida, S., 2008. Estimation of ^{137}Cs plant root uptake using naturally existing ^{133}Cs. J. Nucl. Sci. Technol. 45, 146–151. https://doi.org/10.1080/00223131.2008.10875997.

Lago, D.C., Sánchez, A.D., Prado, M.O., 2022. Cesium immobilization in porous silica and ^{137}Cs self-heating simulations. J. Nucl. Mater. 565, 153697 https://doi.org/10.1016/j.jnucmat.2022.153697.

Komljenović, M., Tanasijević, G., Džunuzović, N., Provis, J.L., 2020. Immobilization of cesium with alkali-activated blast furnace slag. J. Haz. Mat. 388, 121765 https://doi.org/10.1016/j.jhazmat.2019.121765.

Lago, D., Kraxner, J., Galusek, D., Bernardo, E., 2023. Novel glass-based membranes for Cu adsorption: from alkali activation to sintering. Heliyon 9 (8), e18221. https://doi.org/10.1016/j.heliyon.2023.e18221.

Lancellotti, I., Catauro, M., Ponzoni, C., Bollino, F., Leonelli, C., 2013. Inorganic polymers from alkali activation of metakaolin: effect of setting and curing on structure. J. Solid State Chem. 200, 341–348. https://doi.org/10.1016/j.jssc.2013.02.003.

Li, L., Xu, Z., Li, H., Li, J., Hu, D., Xiang, Y., Han, L., Peng, X., 2022. Immobilization of strontium and cesium by aluminosilicate ceramics derived from metakaolin geopolymer-zeolite A composites via 1100 °C heating treatment. Ceram. Int. 48 (11), 15236–15242. https://doi.org/10.1016/j.ceramint.2022.02.054.

Liu, J., Fan, J., Zhang, Y., Miao, J., Cheng, M., Yao, A., Jing, Z., 2021. Hydrothermal conversion of analcime-pollucite solid solution from soil for immobilization of Cs in

situ and its characterization. Mater. Res. Express 8 (9). https://doi.org/10.1088/2053-1591/ac26f4.
Liu, Y., Shi, C., Zhang, Z., Li, N., 2019. An overview on the reuse of waste glasses in alkali-activated materials. Resour. Conserv. Recycl. 144, 297–309. https://doi.org/10.1016/j.resconrec.2019.02.007.
Majérus, O., Lehuédé, P., Biron, I., Alloteau, F., Narayanasamy, S., Caurant, D., 2020. Glass alteration in atmospheric conditions: crossing perspectives from cultural heritage, glass industry, and nuclear waste management. Npj Mate. Degrad. 4 (1), 27. https://doi.org/10.1038/s41529-020-00130-9.
Mehta, A., Karbouche, K., Kraxner, J., Elsayed, H., Galusek, D., Bernardo, E., 2022. Upcycling of pharmaceutical glass into highly porous ceramics: from foams to membranes. Materials 15 (11), 3784. https://doi.org/10.3390/ma15113784.
Ojovan, M.I., Lee, W.E., Kalmykov, S.N., 2019. An Introduction to Nuclear Waste Immobilisation, third ed. Elsevier, Amsterdam, The Netherlands.
Ojovan, M.I., Petrov, V.A., Yudintsev, S.V., 2021. Glass crystalline materials as advanced nuclear wasteforms. Sustainability 13 (8), 4117. https://doi.org/10.3390/su13084117.
Omerašević, M., Lukić, M., Savić-Biserčić, M., Savić, A., Matović, L., Baščarević, Z., Bučevac, D., 2020. Permanent disposal of Cs ions in the form of dense pollucite ceramics having low thermal expansion coefficient. Nucl. Eng. Technol. 52 (1), 115–122. https://doi.org/10.1016/j.net.2019.07.001.
Omerašević, M., Matović, L., Ružić, J., Golubović, Ž., Jovanović, U., Mentus, S., Dondur, V., 2016. Safe trapping of cesium into pollucite structure by hot-pressing method. J. Nucl. Mater. 474, 35–44. https://doi.org/10.1016/j.jnucmat.2016.03.006.
Pomponi, F., Hart, J., 2021. The greenhouse gas emissions of nuclear energy – life cycle assessment of a European pressurized reactor. Appl. Energy 290, 116743. https://doi.org/10.1016/j.apenergy.2021.116743.
Provis, J.L., 2014. Geopolymers and other alkali activated materials: why, how, and what? Materials and Structures/Materiaux et Constructions 47 (1–2), 11–25. https://doi.org/10.1617/s11527-013-0211-5.
Ramteke, D.D., Hujova, M., Kraxner, J., Galusek, D., Romero, A.R., Falcone, R., Bernardo, E., 2021. Up-cycling of 'unrecyclable' glasses in glass-based foams by weak alkali-activation, gel casting and low-temperature sintering. J. Clean. Prod. 278, 123985.
Ray, A., Tiwari, A.N., 2001. Compaction and sintering behaviour of glass-alumina composites. Mater. Chem. Phys. 67 (1–3), 220–225. https://doi.org/10.1016/S0254-0584(00)00443-0.
Rietveld, H.M., 1969. A profile refinement method for nuclear and magnetic structures. J. Appl. Crystallogr. 2 (2), 65–71. https://doi.org/10.1107/s0021889869006558.
Sotelo-Piña, C., Aguilera-González, E.N., Martínez-Luévanos, A., 2019. Geopolymers: past, present, and future of low carbon footprint eco-materials. Handbook of Ecomaterials 4, 2765–2785. https://doi.org/10.1007/978-3-319-68255-6_54.
Tameni, G., Cammelli, F., Elsayed, H., Stangherlin, F., Bernardo, E., 2022. Upcycling of boro-alumino-silicate pharmaceutical glass in sustainable construction materials. Detritus 20, 17–21. https://doi.org/10.31025/2611-4135/2022.15218.
Tian, Q., Bai, Y., Pan, Y., Chen, C., Yao, S., Sasaki, K., Zhang, H., 2022. Application of geopolymer in stabilization/solidification of hazardous pollutants: a review. Molecules 27 (14). https://doi.org/10.3390/molecules27144570.
Wang, J., Zhuang, S., 2020. Cesium separation from radioactive waste by extraction and adsorption based on crown ethers and calixarenes. Nucl. Eng. Technol. 52 (2), 328–336. https://doi.org/10.1016/j.net.2019.08.001.
Wu, Y., Lee, C.P., Mimura, H., Zhang, X., Wei, Y., 2018. Stable solidification of silica-based ammonium molybdophosphate by allophane: application to treatment of radioactive cesium in secondary solid wastes generated from Fukushima. J. Hazard Mater. 341, 46–54. https://doi.org/10.1016/j.jhazmat.2017.07.044.
Xiang, Y., Li, J., Hou, L., Lu, Z., 2021. Rapid transformation from Cs-geopolymers to Cs-defined ceramics by microwave sintering. Ceram. Int. 47 (23), 33089–33097. https://doi.org/10.1016/j.ceramint.2021.08.210.
Xiao, R., Huang, B., Zhou, H., Ma, Y., Jiang, X., 2022. A state-of-the-art review of crushed urban waste glass used in OPC and AAMs (geopolymer): progress and challenges. Clean. Mater. 4, 100083 https://doi.org/10.1016/j.clema.2022.100083.
Xiao, R., Ma, Y., Jiang, X., Zhang, M., Zhang, Y., Wang, Y., Huang, B., He, Q., 2020. Strength, microstructure, efflorescence behavior and environmental impacts of waste glass geopolymers cured at ambient temperature. J. Clean. Prod. 252, 119610 https://doi.org/10.1016/j.jclepro.2019.119610.
Yang, J.H., Han, A., Yoon, J.Y., Park, H.S., Cho, Y.Z., 2017. A new route to the stable capture and final immobilization of radioactive cesium. J. Hazard Mater. 339, 73–81. https://doi.org/10.1016/j.jhazmat.2017.05.062.
Yang, Y., Wang, T., Zhang, Z., Ke, Z., Shan, C., Cao, X., Ma, L., Peng, S., 2020. A novel method to convert Cs-polluted soil into pollucite-base glass-ceramics for Cs immobilization. Chem. Eng. J. 385, 123844 https://doi.org/10.1016/j.cej.2019.123844.
Zhen-Wu, B.Y., Prentice, D.P., Simonetti, D., Ryan, J.V., Sant, G., Bauchy, M., 2021. Predicting zeolites' stability during the corrosion of nuclear waste immobilization glasses: comparison with glass corrosion experiments. J. Nucl. Mater. 547, 152813 https://doi.org/10.1016/j.jnucmat.2021.152813.
Zou, C., Xiong, B., Xue, H., Zheng, D., Ge, Z., Wang, Y., Jiang, L., Pan, S., Wu, S., 2021. The role of new energy in carbon neutral. Petrol. Explor. Dev. 48 (2), 480–491. https://doi.org/10.1016/S1876-3804(21)60039-3.